Supplemental Material

# Molecular Dynamics Investigation of $Cl^-$ and Water Transport through a Eukaryotic CLC Transporter

Mary Hongying Cheng and Rob D. Coalson

Department of Chemistry, University of Pittsburgh

Pittsburgh, PA 15260

# Supplemental Material

## SI Methods

### Simulation systems

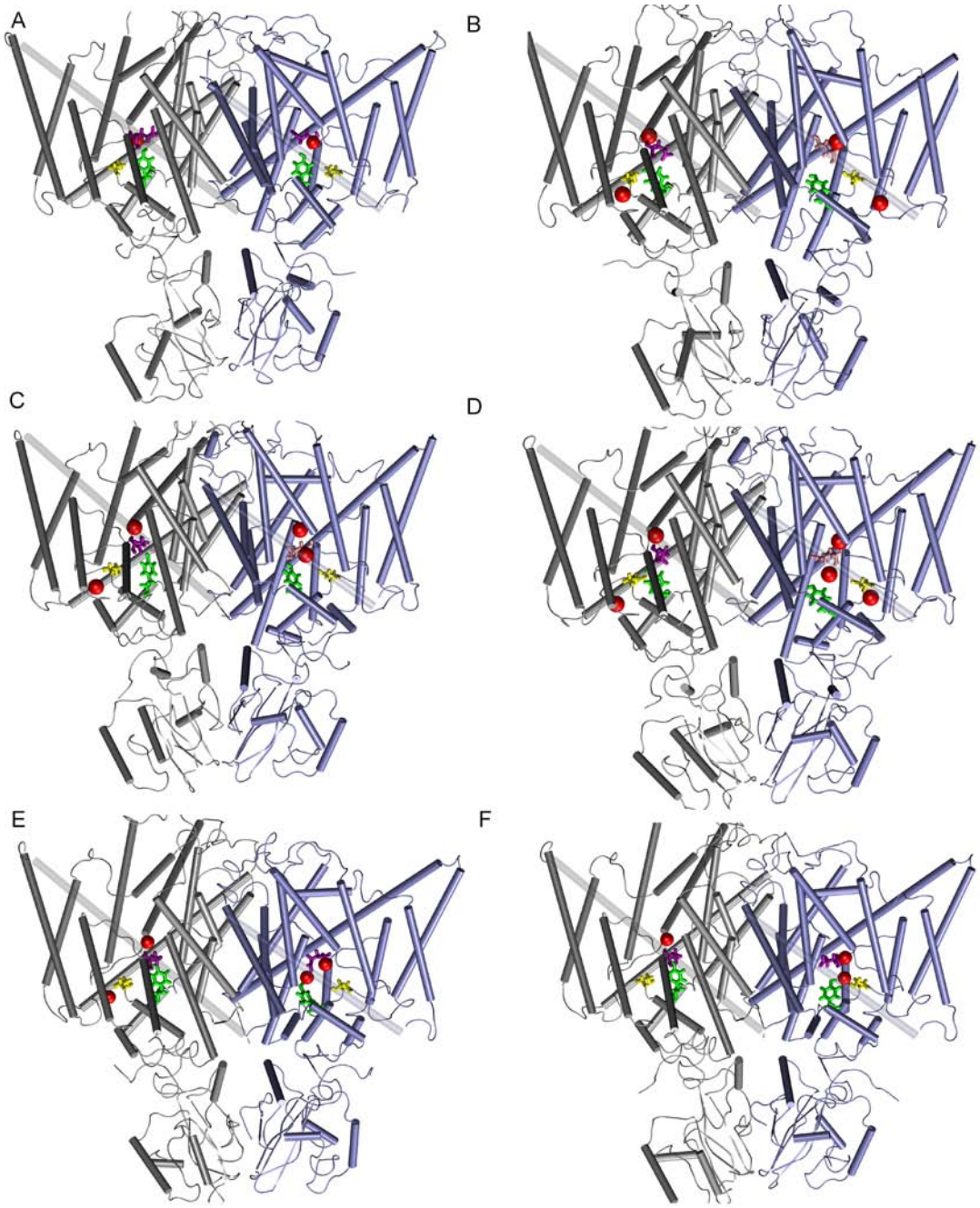


**Fig. S1**: Initial configurations for MD simulation A) System 3; B) System 4; C) System 5; D) System 6; E) System 7; and F) System 8. Y515 and S165 are colored in green and yellow, respectively. Protonated and deprotonated E210 are colored in pink and purple, respectively. Binding $Cl^-$ ions are colored in red. The channel z axis runs from extracellular to intracellular side. In all plots, extracellular region is at top of plot, and intracellular region is at the bottom.

# Supplemental Material

**MD simulation protocols**

Simulations were carried out using NAMD (1) following standard MD procedure. Simulation protocols included periodic boundary conditions, water wrapping, hydrogen atoms constrained via SHAKE, and evaluation of long-range electrostatic forces via the Particle Mesh Ewald (PME) algorithm (2). The bonded interactions and the short-range non-bonded interactions were calculated at every time-step (2 fs), and electrostatic interactions were calculated every two time-steps (4 fs). The cutoff distance for non-bonded interactions was 12 Å. A smoothing function was employed for the van der Waals interactions at a distance of 10 Å. The pair-list of the nonbonded interactions was calculated every 20 time-steps with a pair-list distance of 13.5Å.

**Adaptive biasing force calculations**

The single ion potential of mean force (PMF) profiles for transporting a $Cl^-$ ion from $S_{ext}$ to $S_{cen}$ and $S_{int}$ were calculated along the transport path using the adaptive biasing force (ABF) (3, 4) method implemented in NAMD (1). The ABF calculations of the PMF were carried out in different windows along the ion transport path. The length of each ABF window was 2.0 Å. The initial configurations for each ABF window were either taken from snapshots of our control MD simulations that have the target ion positioned within the window, or obtained from a 100ps equilibration simulation that had the target ion positioned within the window. ABF calculations of the PMF were continued for 6~8 ns within each window. The average force acting on the target ion was accumulated in 0.1 Å sized bins. The boundary force constant was set to be 20 Kcal/mol. The biasing force was applied only after the accumulation of 1000 samples (successive simulation time steps) in individual bins.

## SII Results and Discussion

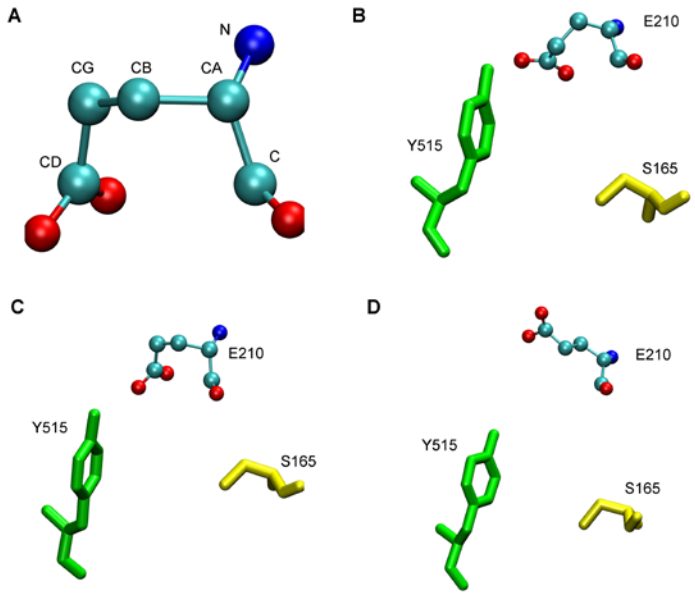


**Fig. S2**: (A) Orientation of the $GLU_{ex}$ gate E210 in the x-ray crystal structure. The $GLU_{ex}$ gate is characterized by two dihedral angles $\chi1$=49.6° (defined by N CA CB and CG atoms) and $\chi2$=90.8° (defined by CA CB CG and CD atoms; B) typical orientation of $\chi1$=80±20° and $\chi2$= -65±20° in subunit A of System $A_dB_d$; C) typical orientation of $\chi1$=50±20° and $\chi2$= 80±20° in subunit B of System $A_dB_d$; (D) typical orientation of $\chi1$= 180° and $\chi2$= 180° for the protonated E210 in System $A_pB_p$. For E210, blue, cyan and red represent nitrogen, carbon and oxygen atoms, respectively. Hydrogen atoms are not shown in the figures.

# Supplemental Material

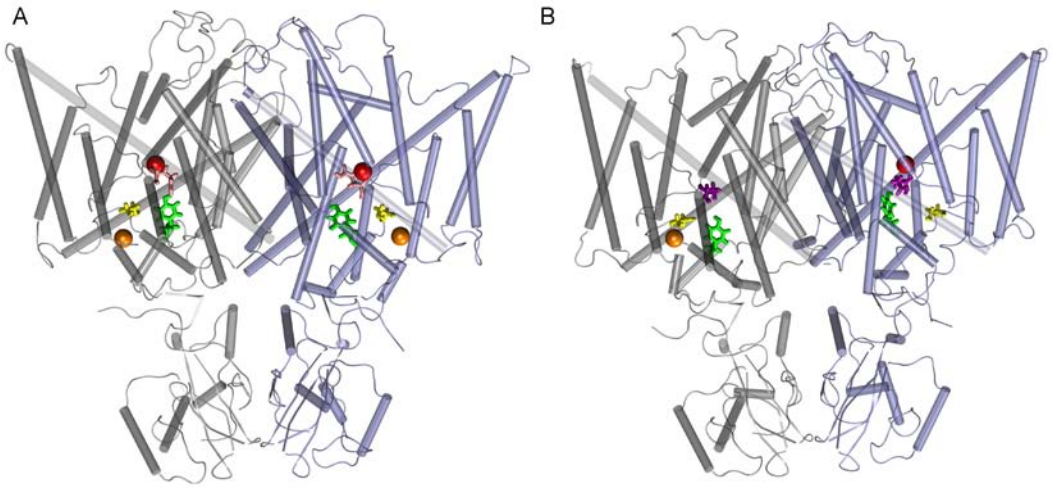


**Fig. S3**: Comparison of CmCLC after 80 ns MD simulations with (A) protonated E210 ($A_pB_p$ system); and (B) deprotonated E210 ($A_dB_d$ system). Channel orientation is the same as in Fig. 1. Red and orange balls represent $Cl^-$ ions in the crystal structure and coming from the internal solution, respectively. Protonated and deprotonated E210 are colored in pink and purple, respectively. In our simulations, $Cl^-$ ions which originally occupied the $S_{int}$ sites in the X-ray structure escaped to the internal solution within 40 ns in both $A_dB_d$ and $A_pB_p$ simulation systems. After an additional 30 ns of MD simulation, other $Cl^-$ ions migrated from the intracellular solution and occupied the $S_{int}$ sites again. Extracellular region is at top of plot, and intracellular region is at the bottom.

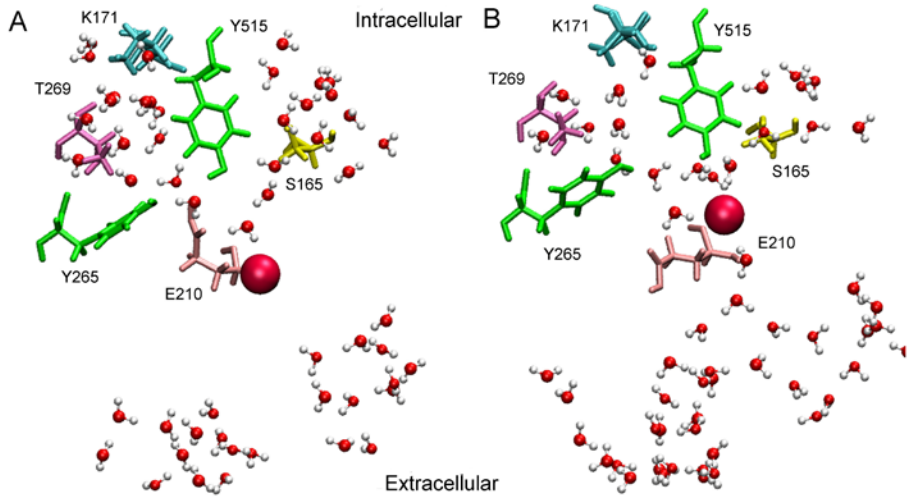


**Fig. S4**: A) Waters within 12 Å of the $GLU_{ex}$ gate (E210) at 80 ns in the $A_pB_p$ system (protonated E210) without external potential. A continuous water wire starting from the intracellular K171 and extending to the $GLU_{ex}$ gate quickly formed and remained stable throughout the simulations. This continuous water path has been previously proposed as the proton transport pathway (5-7). The external binding site $S_{ext}$ is highly hydrophobic, F256 and V431, or P432 and V431 (not shown) can block the water path from the extracellular solution to the $S_{ext}$ site, leading to a dehydrated $Cl^-$ binding to the $S_{ext}$ site for the majority of the 80 ns of MD simulation; B) A continuous water path from the extracellular solution to the $GLU_{ex}$ gate was formed within 4ns once an external potential of -120 mV was applied. Waters are shown in CPK format.

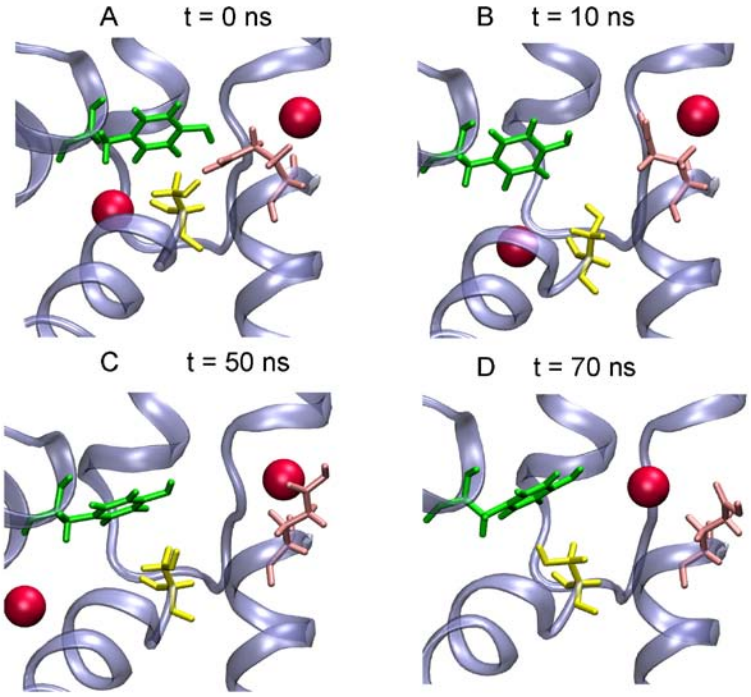


**Fig. S5**: MD snapshots of $A_pB_p$ system at A) t = 0 ns, B) t = 10 ns, C) t = 50 ns and D) t = 70 ns. Residues S165, protonated E210 and Y515 are shown in yellow, pink and green, respectively. Within 50 ns the $GLU_{ex}$ gate swung from the $S_{cen}$ site to the extracellular solution and fully opened for $Cl^-$ transport (C and D).

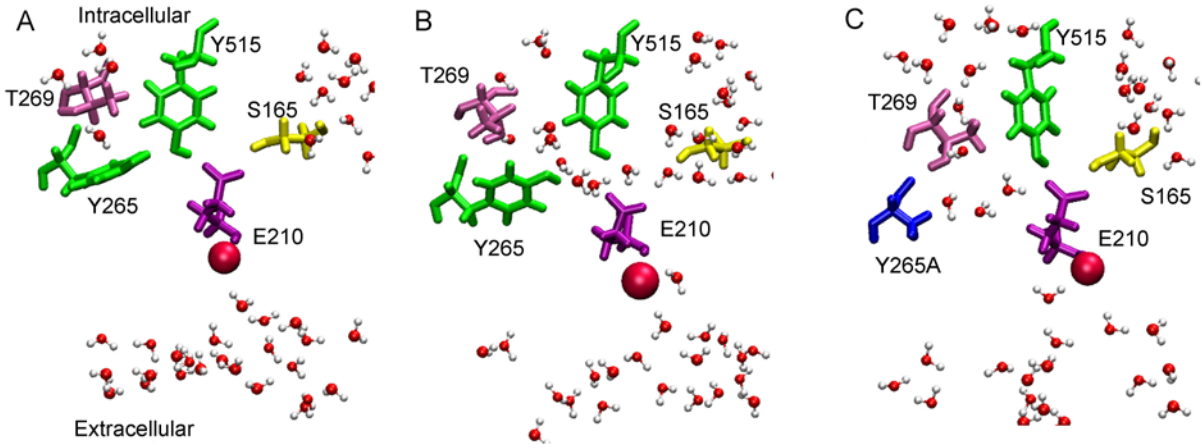


**Fig. S6**: Comparison of waters within 12 Å of the deprotonated $GLU_{ex}$ gate (E210) in A) $A_dB_d$ system; B) System 4; and C) Y265A mutant channel. The deprotonated $GLU_{ex}$ gate is shown in purple. In System 4, the $GLU_{ex}$ gate was deprotonated after a simulation of 80 ns in the $A_pB_p$ system. Y265A mutation was performed on the $A_dB_d$ system.

# Supplemental Material

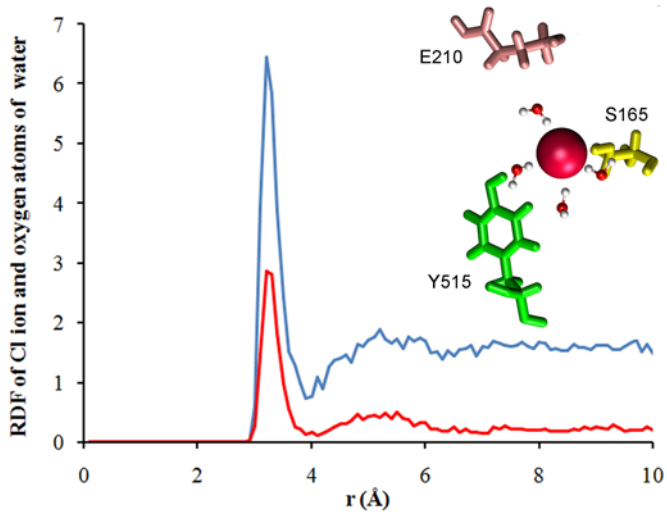


**Fig. S7**: Comparison of the radial distribution function (RDF) of the permeant $Cl^-$ ion and oxygen atoms of water in bulk water solution (blue line) and inside the permeation path lined by Y515 and S165 (red line). More than 50% dehydration of the first hydration shell was observed when the $Cl^-$ was transferred from bulk solution to the location indicated in the inset figure, which shows the permeant $Cl^-$ with its first hydration shell in the constriction formed by Y515 and S165.

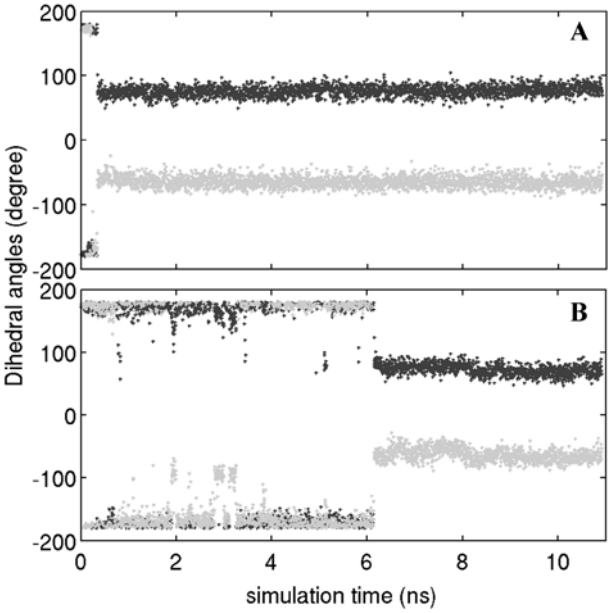


**Fig. S8:** Time evolution of dihedral angles χ1 (black) and χ2 (gray) of the $GLU_{ex}$ gate in (A) subunit A and (B) subunit B of System 3. Once initially protonated E210 was deprotonated, dihedral angles of χ1 and χ2 changed from initial values ±180°±20° to the values 70°±20° and -65°±15°. The orientation change of the $GLU_{ex}$ gate facilitated the translocation of $Cl^-$ from the $S_{cen}$ to the $S_{int}$ site.

# Supplemental Material

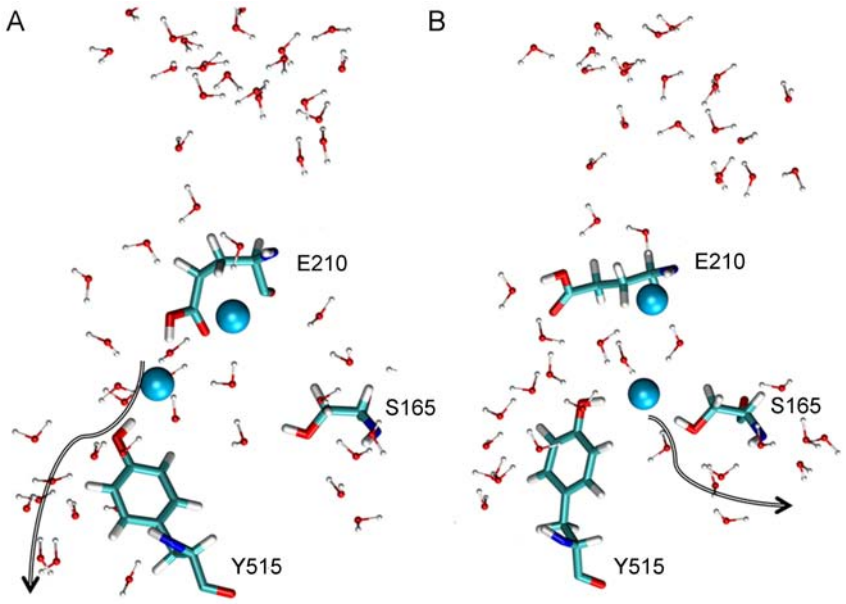


**Fig. S9**: Binding of two $Cl^-$ ions (cyan spheres) to the $S_{cen}$ site when E210 is protonated. One $Cl^-$ ion binds near the backbone of the $GLU_{ex}$ gate and the other either binds to A) a site lined by the hydroxyl groups from Y515 and E210 (termed site A); or B) a site lined by the hydroxyl groups from Y515 and S165 (termed site B). Extracellular region is at top of plot, and intracellular region is at the bottom. Black arrows illustrate putative $Cl^-$ paths found in our simulations.

## Supporting References:


1. Phillips, J. C., R. Braun, W. Wang, J. Gumbart, E. Tajkhorshid, E. Villa, C. Chipot, R. D. Skeel, L. Kale, and K. Schulten. 2005. Scalable molecular dynamics with NAMD. *J Comput Chem* 26:1781-1802.
2. Darden, T., D. York, and L. Pedersen. 1993. Particle Mesh Ewald - an N.Log(N) Method for Ewald Sums in Large Systems. *J Chem Phys* 98:10089-10092.
3. Darve, E., D. Rodriguez-Gomez, and A. Pohorille. 2008. Adaptive biasing force method for scalar and vector free energy calculations. *J Chem Phys* 128:144120.
4. Chipot, C., and J. Hénin. 2005. Exploring the free-energy landscape of a short peptide using an average force. *J Chem Phys* 123: 244906.
5. Wang, D., and G. A. Voth. 2009. Proton transport pathway in the ClC $Cl^-/H^+$ antiporter. *Biophys J* 97:121-131.
6. Kieseritzky, G., and E. W. Knapp. 2011. Charge transport in the ClC-type chloride-proton anti-porter from Escherichia coli. *J Biol Chem* 286:2976-2986.
7. Kuang, Z. F., U. Mahankali, and T. L. Beck. 2007. Proton pathways and $H^+/Cl^-$ stoichiometry in bacterial chloride transporters. *Proteins: Struct., Func., and Bioinform* 68:26-33.